Effects of biologically induced differential heating in an eddy-permitting coupled ocean-ecosystem model

Ulrike Löptien,[1] Carsten Eden,[1] Axel Timmermann,[2] and Heiner Dietze[3]

[1] On the basis of integrations of an eddy-permitting coupled physical-biological model of the tropical Pacific we explore changes in the simulated mean circulation as well as its intraseasonal to interannual variability driven by the biologically modulated vertical absorption profiles of solar radiation. Three sensitivity ocean hind-cast experiments, covering the period from 1948 to 2003, are performed. In the first one, simulated chlorophyll affects the attenuation of light in the water column, while in the second experiment, the chlorophyll concentration is kept constant in time by prescribing an empirically derived spatial pattern. The third experiment uses a spatially and temporally constant value for the attenuation depth. The biotically induced differential heating is generated by increased absorption of light in the surface layers, leading to a surface warming and subsurface cooling. The effect is largest in the eastern equatorial Pacific. However, the initial vertical redistribution of heat leads to considerable changes of the near-surface ocean circulation subsequently influencing the near-surface temperature structure. In general, including biophysical coupling improves the model performance in terms of temperature and ocean circulation patterns. In particular, the upwelling in the eastern equatorial Pacific is enhanced, the mixed layer becomes shallower, the warm bias in the eastern Pacific is reduced, and the zonal temperature gradient increases. This leads to stronger La Niña events and an associated increase in the variability of the Niño3 SSTA time series. Furthermore, the eddy kinetic energy (EKE) associated with mesoscale eddies in the eastern equatorial Pacific increases by almost 100% because of enhanced EKE production due to enhanced horizontal and vertical shear of the mean currents.

1. Introduction

[2] The El Nino Southern Oscillation (ENSO) phenomenon is a global mode of natural interannual climate variability affecting the worldwide weather and climate patterns. Our understanding of associated drivers and feedback mechanisms in the tropical Pacific, however, is still limited, a fact epitomized by state-of-the art coupled ocean-atmosphere circulation models, which suffer from biased temperatures and an inadequate representation of intraseasonal to interannual variability [*Bony et al.*, 2007]. One attempt to reduce such biases endemic to coupled models was explored by *Timmermann and Jin* [2002] who included climate-state–dependent chlorophyll concentrations in a simplified coupled ocean-atmosphere model. Their results

implied that the variable chlorophyll concentration affects the mean state as well as ENSO variability. Chlorophyll and related pigments in phytoplankton strongly absorb light in the blue and red parts of the spectrum and can thereby modify the vertical distribution of radiant heating which results in enhanced surface warming and subsurface cooling [*Lewis et al.*, 1983, 1990; *Sathyendranath et al.*, 1991]. A 10 W/m^2 change in solar radiation absorbed within the mixed layer can result in a temperature change of more than 0.6 K/month [*Ohlmann et al.*, 2000]. This effect is especially important in the tropical Pacific since here, shortwave radiation is strong. Additionally, equatorial upwelling supplies nutrients, giving rise to a chlorophyll maximum at the equator, while the chlorophyll concentration is low elsewhere in the region. Thus the spatial chlorophyll variability is large leading to strong spatial differences in the light attenuation. Moreover, the ocean biology in the tropical Pacific is strongly influenced by seasonal to interannual climate variations, in particular by El Niño/La Niña transitions [*Lengaigne et al.*, 2007]. During La Niña conditions, the shallow thermocline and nutricline intersect with the euphotic zone, thereby enhancing biological productivity. El Niño conditions, on the other hand, are typically related to a depressed thermocline in the eastern equatorial Pacific and thus associated with

---

[1]Ozeanzirkulation und Klimadynamik, Leibniz-Institut für Meereswissenschaften, Kiel, Germany.
[2]International Pacific Research Center, School of Ocean and Earth Science and Technology, University of Hawai'i at Manoa, Honolulu, Hawaii, USA.
[3]Marine Biogeochemie, Leibniz-Institut für Meereswissenschaften, Kiel, Germany.

reduced rates of nutrient supply, primary production and chlorophyll concentrations [e.g., *Pennington et al.*, 2006].

[3] In summary, the influence of chlorophyll on the radiant heating of the water column and potential changes of ocean dynamics can be assumed to be particularly large in the tropical Pacific. While differing in the details, other studies [*Anderson et al.*, 2007, 2009; *Gnanadesikan and Anderson*, 2009; *Marzeion et al.*, 2005; *Nakamoto et al.*, 2001; *Manizza et al.*, 2005; *Murtugudde et al.*, 2002; *Lengaigne et al.*, 2007; *Sweeney et al.*, 2005; *Wetzel et al.*, 2006; *Zhang et al.*, 2009] confirmed the general finding that biotically induced differential heating has a significant effect on the tropical Pacific climate, and its interannual variability (ENSO) in ocean only as well as in coupled experiments. Observational studies further support the general notion of a biotic influence on tropical Pacific climate [*Lewis et al.*, 1990; *Sathyendranath et al.*, 1991; *Strutton and Chavez*, 2004]. However, the details of this bioclimate coupling seem to be highly model-dependent and have not been fully resolved yet.

[4] To explore these interactions, recent studies have employed coarse-resolution ocean models that neglect the potential of intraseasonal or mesoscale eddy variability on nutrient supply and ocean biota. In this study we use an eddy-permitting ocean model that is coupled to a simple pelagic ecosystem model. It is known that, for instance, Tropical Instability Waves (TIWs), unresolved in previous studies, strongly affect chlorophyll concentrations [*Strutton and Chavez*, 2004] and the associated absorption of solar radiation. Further, eddy activity may also play a role in modulating the effect of ocean biota on tropical Pacific climate by, for instance, the modulations of the strength of the TIWs on intraseasonal to interannual timescales by ENSO [*Vialard et al.*, 2003]. Thus increasing the resolution might lead to new insights which cannot be obtained by coarser resolution models.

[5] The paper is organized as follows: section 2 is composed of a description of the model and experimental setups. Section 3 discusses the ability of the model to simulate the chlorophyll concentration in the tropical Pacific and compares the simulations with observations. Section 4 describes the influence of chlorophyll on the climate mean state in the tropical Pacific. Sections 5 and 6 discuss the influence of chlorophyll on driving variability in the physical model, focusing on interannual variability in section 5 and on the intraseasonal variability in section 6. A summary of the main results and a discussion of their relevance is given in section 7.

2. Model Description and Experiments

[6] The present study is based on integrations conducted with a regional eddy-permitting model. The model domain is composed of the tropical Pacific Ocean from 30°N to 30°S and 100°E to 90°W with open boundaries [*Stevens*, 1990] in the north, south and west of the domain. The vertical grid is a z-level grid with 42 vertical levels with thicknesses ranging from 10 m near the surface to 250 m at the deepest level of 5500 m. The upper 300 m contain 12 vertical layers. The numerical code is a rewritten version of the GFDL MOM-2.1 code [*Pacanowski*, 1992] and can be found at http://www.ifm-geomar.de/∼spflame. We use a

rigid lid formulation for the external mode for which the barotropic stream function (derived from the ECCO data set [*Koehl et al.*, 2006]) is prescribed at the open boundaries. Biharmonic horizontal mixing and friction with a diffusivity of 7.9×10^{14} m^4/s is used. Vertical mixing is parameterized using the TKE scheme of *Gaspar et al.* [1990]. The ocean circulation model is driven by climatological monthly mean forcing in a 30 yearlong spin-up period to allow for a dynamical adjustment of the circulation. The net heat fluxes and the climatological wind stress are derived from an analysis of the ECMWF weather forecast model [*Barnier et al.*, 1995]. For the heat flux forcing a Haney-type [*Haney*, 1971] boundary condition is used, that is, a spatially and monthly varying restoring term is added to the heat flux forcing (following that of *Barnier et al.* [1995]). The restoring terms are reaching maximum values of 25 W/m^2/K in the tropics and somewhat higher values in the subtropics. For sea surface salinity we apply a restoring boundary condition using the climatology by *Levitus et al.* [1994] which also provides the initial condition and lateral boundary values at open boundaries in case of inflow conditions. Initial conditions and boundary values for nitrate are those from the *Conkright et al.* [1994] climatology while the initial conditions of the organic compartments of the ecosystem model are set close to zero.

[7] After the first 30 year spin-up period, the circulation model is coupled online to a simple pelagic ecosystem model and run for another 30 years allowing for an adjustment of the biogeochemical variables within the main thermocline. The ecosystem model, consists of four compartments, namely nitrate, phytoplankton, zooplankton and detritus (a so-called NPZD model). Note that chlorophyll is not a prognostic variable but is diagnosed from phytoplankton concentrations assuming a constant ratio of 1.59 mgChl/mmol N. Biotic sources and sinks of the respective compartments, as well as the associated parameters are identical to settings in the study by *Oschlies and Garcon* [1999] except for a reduced saturation growth rate for phytoplankton (by a factor of 20) which is meant to mimic the effect of iron limitation in the tropical Pacific. The effect of this choice on short-term chlorophyll variability will be discussed below. After the spin-up, lasting a total of 60 years, the simulated phytoplankton distribution is allowed to interact with the physical model by changing the vertical solar radiation absorption profile in the surface layers as described in the study by *Marzeion et al.* [2005]. For the case of clear water it is assumed that the penetration below the surface is wavelength-dependent and the energy partitions between two exponentials. 58% of the energy decays with a 35 cm e-folding scale and 42% with a 23 m e-folding scale. These values correspond to a Jerlov's Type I oligotrophic water [*Jerlov*, 1968]. In the presence of chlorophyll the attenuation coefficients for seawater are modified as a function of the chlorophyll concentration using the empirical constants suggested by *Morel* [1988] as described in the study by *Marzeion et al.* [2005]. This formulation does not lead to deeper penetration than Jerlov's Type I water in our model and the solar penetration depth is generally reduced by accounting for chlorophyll in the solar absorption schema. Note, that the light distribution, which affects phytoplankton growth, is not affected by the phytoplankton concentration itself, that is, there is no self-shading effect.
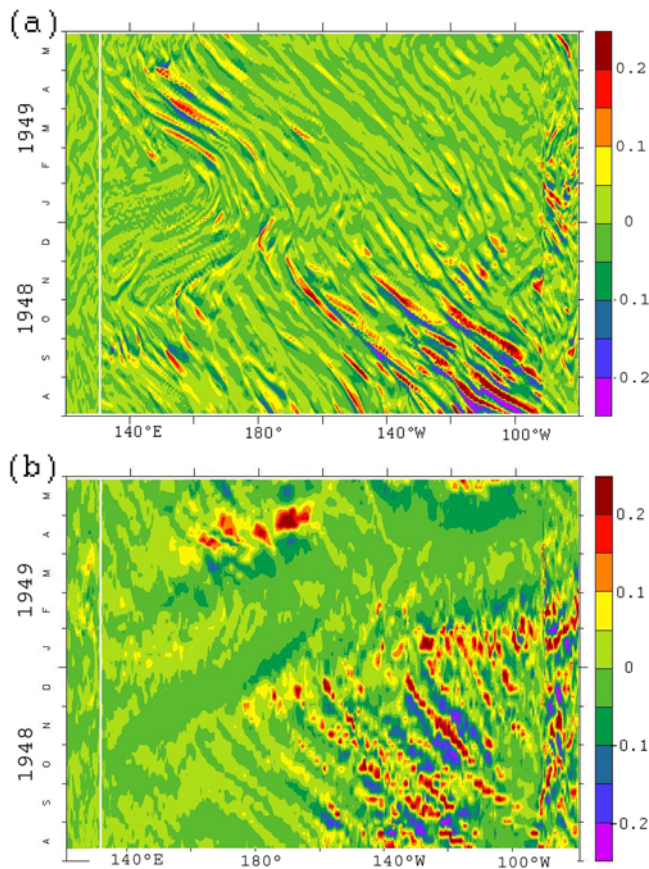
Figure 1. High-pass filtered chlorophyll concentration averaged over the upper 20 m at the equator in mgChl/m^3. Shown are fluctuations lasting shorter than 3 weeks. (a) As simulated with our standard model in the experiment BIO and (b) as simulated in the sensitivity experiment ZOO.

To test the effect of self-shading on modeled phytoplankton concentrations a suite of experiments was integrated in a one-dimensional environment. Several differing sets of boundary and initial conditions representative for the equatorial Pacific were tested. A linear dependence of the light attenuation on phytoplankton concentration with coefficients ranging up to 0.04 m^{-1}/(mmolN/m^3) [*Penta et al.*, 2008, Table 1] revealed that the difference in phytoplankton concentrations modeled with and without accounting for the self-shading was always less than 10%.

[8] After using climatological surface forcing during the 60 years of spin-up, the surface forcing used for the three main experiments discussed in this study was changed to interannually varying monthly mean wind stress from NCEP/ NCAR from 1948–2003 [*Kalnay et al.*, 1996] and monthly mean climatological forcing otherwise (as used during the spin-up period). We find more realistic interannual sea surface temperature (SST) fluctuations in the El Niño region when we neglect varying surface heat flux forcing in the equatorial Pacific of our model. Also, other surface heat flux formulations, such as the one suggested by *Seager et al.* [1995], do not improve the model simulations. This issue is, however, not further discussed in the present paper.

[9] In order to explore the influence of ocean biota on ocean physics we performed three hind-cast experiments (1948–2003) using the NCEP/NCAR wind stress forcing:

in the first experiment an ecosystem model interacts with the physical model as described above (experiment BIO hereafter), in the second experiment (CONSTBIO) the chlorophyll concentration was held constant, using the long-term annual mean pattern from the preceding integration, and in the third experiment (NOBIO) without any chlorophyll. Note that in the third experiment and also during the 60 year spin-up period, we have assumed Jerlov's water type I for the penetration depth of solar radiation.

3. Simulated Chlorophyll Concentration

[10] A prerequisite for our study is a realistic simulation of the chlorophyll distribution in the equatorial Pacific which we discuss in this section. Since the phytoplankton growth was too strong with the standard parameter settings we have reduced the saturation growth rate for phytoplankton by a factor of 20 compared to the standard set of parameters which has been found to be adequate for mid and high latitudes and the equatorial Atlantic Ocean [*Oschlies and Garcon*, 1998, 1999; *Eden and Oschlies*, 2006]. Without this reduction, the NPZD model simulates unrealistically high phytoplankton concentrations in the equatorial Pacific (not shown) which is accompanied by a complete and unrealistic depletion of nitrate at the surface. Since the maximal growth rate of phytoplankton is thus only 0.6/20 days^{-1} in our modified model version, shorter-term phytoplankton blooms such as those that are sometimes observed [*Ryan et al.*, 2006; *Strutton and Chavez*, 2004] cannot be simulated realistically. Moreover, any local, modeled variability of phytoplankton concentrations on timescales shorter than one month must be the result of physical redistribution of phytoplankton by advection or diffusion, rather than driven by ecosystem dynamics. We found that despite the reduced growth rate, the near-surface chlorophyll variability in experiment BIO is quite pronounced on timescales of less than 3 weeks (not shown). This is mainly due to subsurface chlorophyll maxima which are vertically advected to the surface.

[11] To test the model bias potentially introduced by the relatively slow phytoplankton growth in BIO, we integrated an additional experiment, named ZOO. This experiment is identical to the experiment BIO except for the following changes: (1) the original, i.e., more rapid, phytoplankton growth rate of 0.6 days^{-1} (compared to 0.6/20 days^{-1} in BIO) is applied. (2) The parameterization of zooplankton is modified so that zooplankton feeds on both phytoplankton and detritus (whereas in the original version (BIO) zooplankton is not allowed to feed on detritus). The additional parameter describing the preference of zooplankton to feed on detritus is set to 0.37. Consequently, there is a higher zooplankton concentration in ZOO exerting a top-down control on phytoplankton stocks and associated nitrate uptake. Thus the modeled temporal mean phytoplankton and nitrate concentrations are similar to those modeled in the experiment BIO, although controlled by different dynamics. Figure 1 reveals the impact of the revised parameterization on the high-frequency chlorophyll variability. When weighting the variability with the mean vertical maximum of chlorophyll in the Niño3 region, we find similar high-frequency variability in the experiments ZOO and BIO and conclude that the reduced phytoplankton
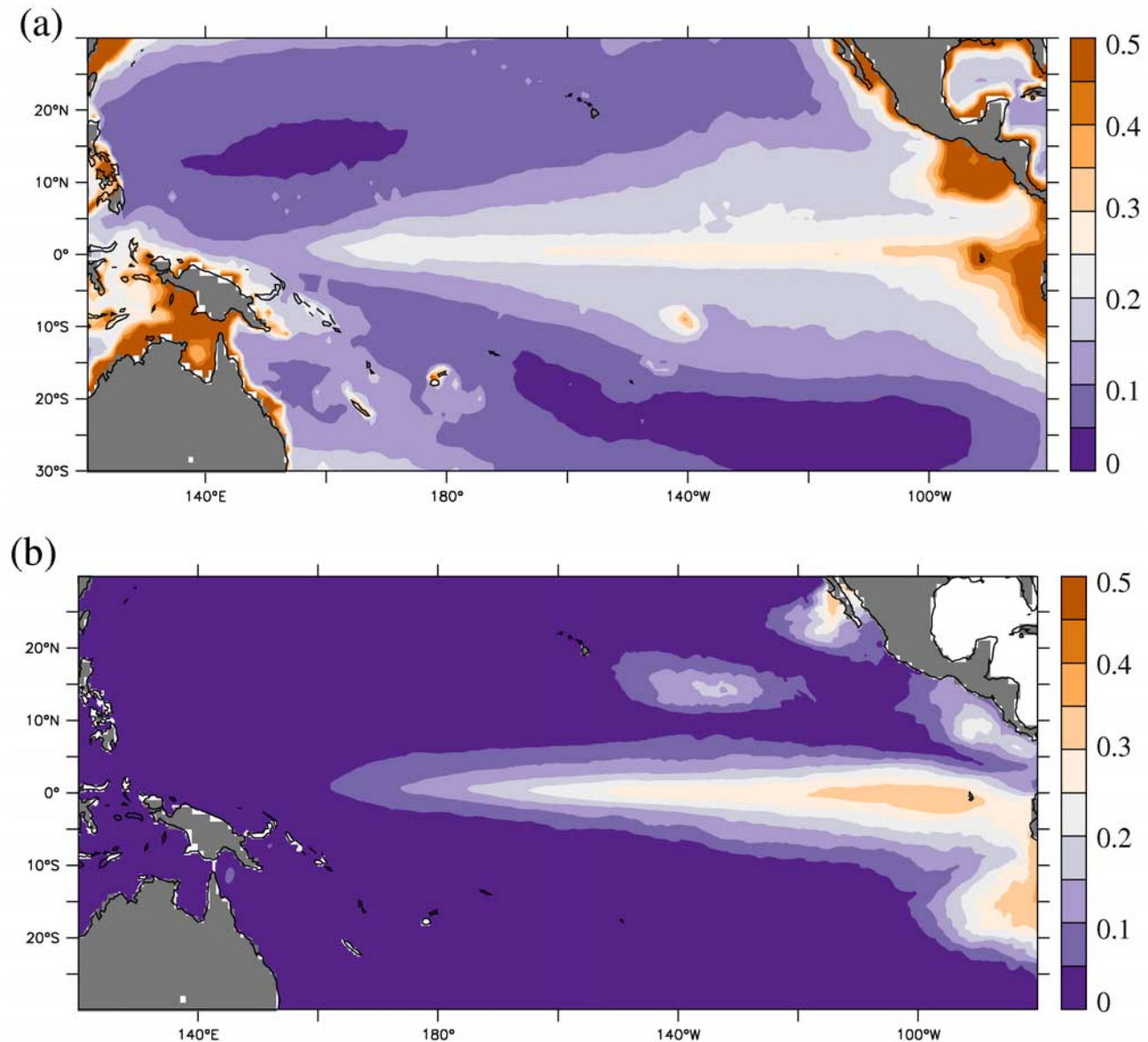
Figure 2. Mean chlorophyll concentration from 1997 to 2001 in mg Chl/m^3 (a) as observed by SeaWIFS and (b) averaged in the upper 20 m for the BIO experiment during the same period.

growth rate tends to be of minor importance for the high-frequency chlorophyll variability and that the effect of vertical advection dominates.

[12] We have no hard proof that this physics correctly represents reality. However, since we are focusing on the effects of chlorophyll on the circulation; we are more concerned with simulating the large-scale, long-term chlorophyll concentrations and not the details of biology. We note, however, that caution must be exercised when focusing on high-frequency physical processes. The simulated large-scale chlorophyll concentration does seem reasonable for our purposes.

[13] Also, we are aware that explicitly resolved iron limitation might change the results but assume, nevertheless, that for our purposes, the model performs sufficiently well under the caveat that caution has to be taken when focusing on high-frequency biological processes. Considering the experiment BIO in the following text the simulated

large-scale chlorophyll concentration seems reasonable for our purposes. Figure 2 shows the mean near-surface chlorophyll distribution in experiment BIO in comparison to observational estimates of chlorophyll concentrations of the Sea-viewing Wide Field-of-view Sensor (SeaWIFS) [*McClain et al.*, 2002, 2004]. Although regional differences are evident, e.g., near the coast where local maxima seen in the satellite observations are not captured well by the model, the simulated large-scale chlorophyll concentrations are sufficiently realistic. Considering the logarithm of observed and modeled chlorophyll leads to a mean correlation of 0.65 and maximum values of 0.78 in the cold tongue region (170°W–90°W, 4°S–4°N). Along the equator, chlorophyll concentrations increase eastward, reaching maxima of 0.3 mg/m^3 near the Galapagos Islands and the coast of South America. The model is not able to reproduce the low chlorophyll concentrations of less than 0.05 mg/m^3 in oligo-
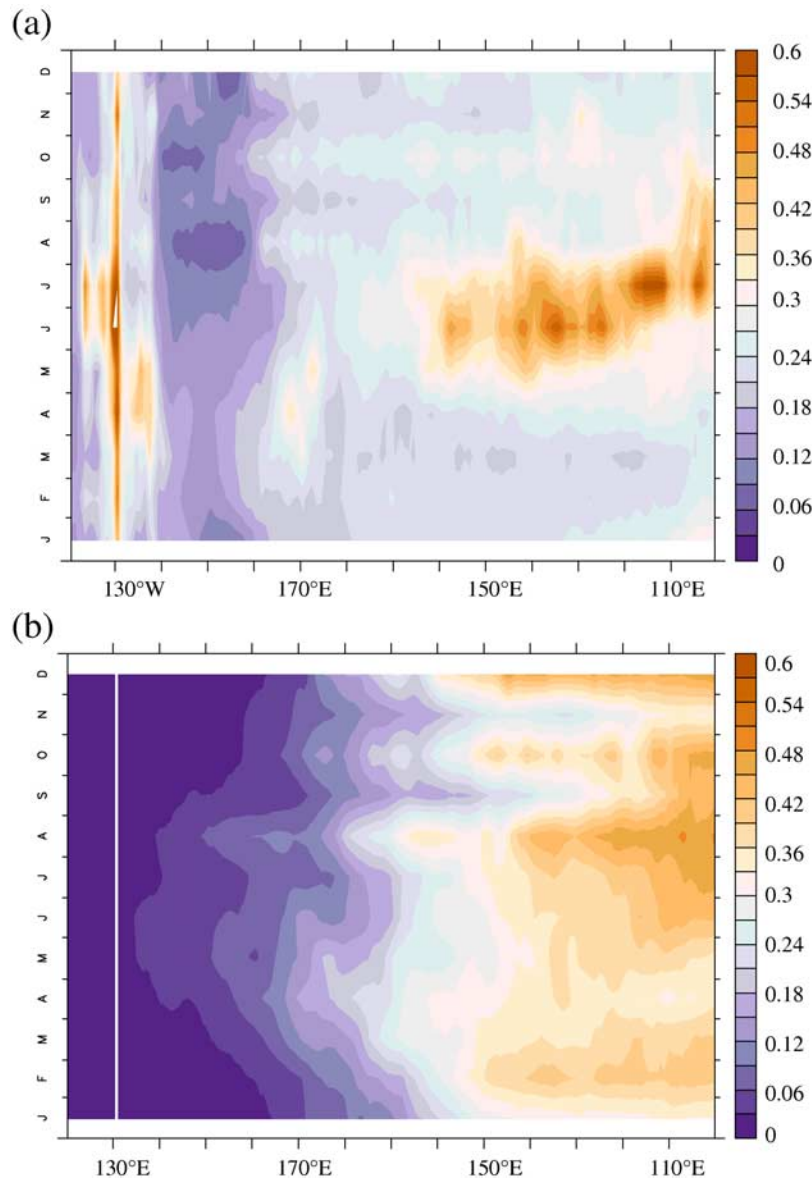
Figure 3. Mean seasonal cycle of the near-surface chlorophyll concentration at the equator (1997–2001) in mgChl/m^3 (a) as observed by SeaWIFS and (b) as simulated in the experiment BIO averaged over the upper 20 m during the same period.

trophic regions, e.g., within the subtropical gyres, where the simulated chlorophyll concentrations tend to be zero.

[14] Figure 3 shows the mean seasonal cycle of near-surface chlorophyll in BIO in comparison to SeaWIFS at the equator for the years 1997–2001 in both model and observations. The seasonal cycle tends to be somewhat too weak compared to observations. The observed chlorophyll concentration at 110°W ranges from 0.23 to 0.6 mg chl/m^3 while the interval from 0.35 to 0.55 mg chl/m^3 in the simulation is considerably smaller. Additionally, the peak of the seasonal cycle in May–June in the satellite data is about one month late in the model simulation. Strong local maxima of chlorophyll concentrations near coasts in the satellite data are, again, not reproduced by the model. Apart from the period during the bloom, too much phytoplankton is simulated in the eastern equatorial Pacific during the year. This is especially true during the winter months where

the modeled chlorophyll is almost doubled compared to the satellite observations. On the other hand, the strength of the summer bloom is well reproduced.

[15] As described above, a large contribution of interannual chlorophyll variability can be associated with ENSO. This difference between El Niño and La Niña years is well captured by the model as shown in Figure 4 even though the simulated difference between La Niña and "normal" years is too weak. The RMS of the observed monthly mean chlorophyll concentration in the Nino3 region is 0.035 (mg chl/m^3) compared to 0.042 (mg chl/m^3) in our simulation. During the strong El Niño 1997/1998 the chlorophyll concentration around the equator (10°S–10°N) is very low in Figures 4a and 4b, model and observations, while the subsequent strong bloom in the observational data is only partly captured (i.e., with smaller magnitude) by the model. Note also, that
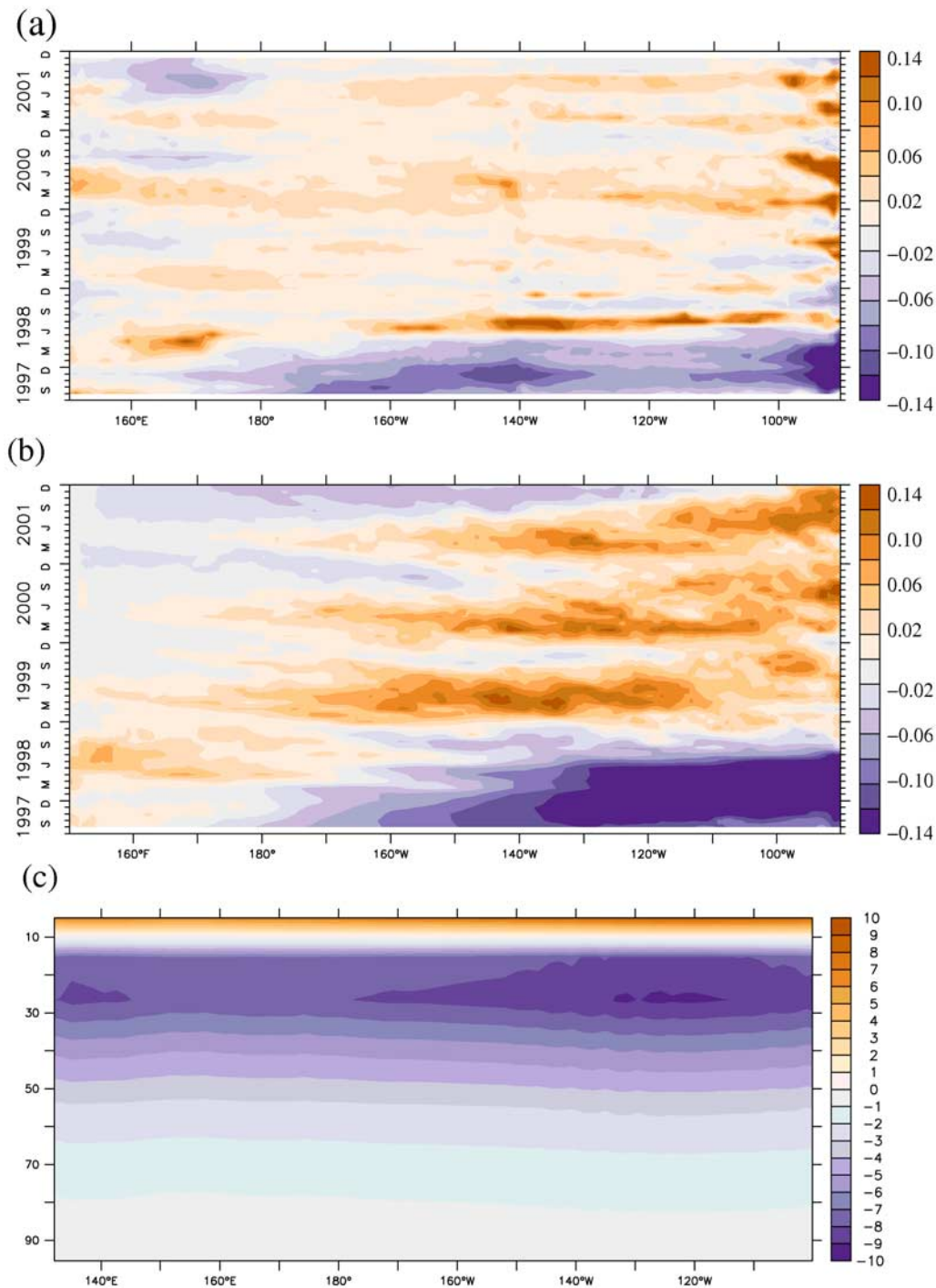
Figure 4. Anomalous near-surface chlorophyll concentration in mgChl/m^3 along the equator averaged from $10°S–10°N$ (a) as observed by SeaWIFS and (b) as simulated in the experiment BIO averaged over the upper 20 m. (c) Mean difference of the heating at the equator between the experiments BIO and NOBIO (1948–2001) rates in Kelvin per year.

the mean near-surface chlorophyll distribution prescribed in CONSTBIO is very similar to the chlorophyll concentration in Figure 2.

[16] The observed vertical distribution of chlorophyll in the equatorial Pacific features large subsurface maxima, which we also find in our simulation. The importance of those subsurface maxima for solar absorption and their bio-optical effects were already discussed by, e.g., *Marzeion et al.* [2005] and *Murtugudde et al.* [2002]. In our model the difference between surface and subsurface chlorophyll concentration is most pronounced during El Niño years (not shown) with equatorial subsurface maxima occurring at a depth of 80 m (not shown). Comparing the simulated vertical chlorophyll distribution with observational estimates by *Aufdenkampe et al.* [2002] and *Pennington et al.* [2006] reveals that the simulated subsurface maxima exhibit
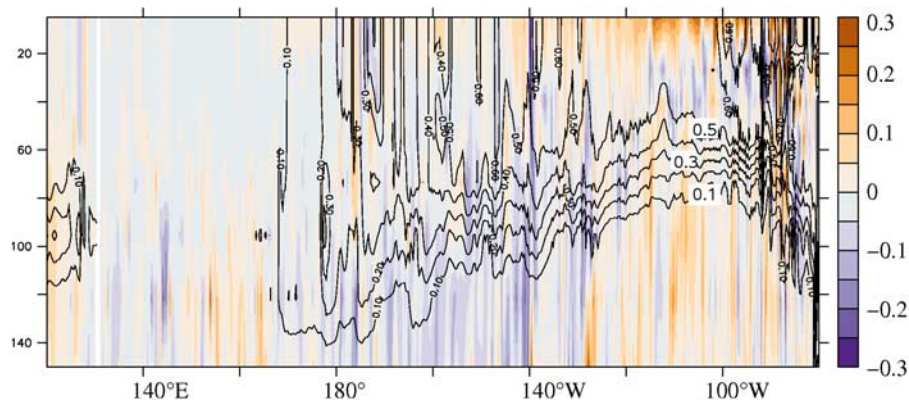
Figure 5. Temperature difference (in Kelvin) between the experiments BIO and NOBIO plotted along the equator averaged over the first 6 days of the hindcast simulation following the spin-up period. The contour lines depict the corresponding chlorophyll concentrations in mg chl/m^3.

realistic depth and magnitude (not shown). *Aufdenkampe et al.* [2002] observe strong chlorophyll maxima in a depth of 60–70 m during a cruise along the equator in April 1996. When considering the simulated monthly mean chlorophyll during this month our simulation shows a maximum of similar order of magnitude, although situated 5–10 m deeper. The major difference compared to the simulated section is the smaller spatial extent of the observed subsurface maxima. However, *Aufdenkampe et al.* [2002] consider a synoptic zonal ship section, while we compare the simulated monthly mean chlorophyll along the equator such that the observed small-scale features cannot be expected to be reproduced exactly by the model. On the other hand, *Pennington et al.* [2006] averaged several meridional ship sections across the equator from September 1997–May 2005 in the eastern equatorial Pacific which compares well with the mean (1998–2003) simulated chlorophyll distribution averaged from 130°W to 140°W. The maximum chlorophyll is obtained in the vicinity of the equator in a depth of 60–70 m in both model and observations peaking at 0.3 mg chl/m^3 and ranging from 15°S and 15°N.

4. Biologically Induced Changes in the Mean State

[17] We have diagnosed the changes in the mean heating rates due to the shortwave absorption by chlorophyll. A pronounced surface warming in the upper 10 m of 0.3–1 K/month shows up in the presence of chlorophyll in BIO compared to NOBIO, which amounts to 15–20% of the heating rates in NOBIO. In contrast (and as a consequence), the deeper layers stay cooler in BIO. Since the maximum of chlorophyll occurs at the equator the effect on the heating rates is strongest there. Figure 4c shows the differences in the mean heating rates between the experiments BIO and NOBIO at the equator. The surface warming and subsurface cooling is most pronounced in the eastern Pacific, since the chlorophyll concentrations are largest here. A local minimum of the cooling occurs at a depth of 15–30 m. In contrast, the differences in the solar heating rates in BIO and CONSTBIO result only from nonlinearities in the formulation of the solar absorption schema and are accordingly rather small (not shown).

[18] To further investigate the effect of shortwave absorption due to chlorophyll concentrations, we consider the differences in the simulated mean states in BIO, CONSTBIO and NOBIO. The initial response to biologically induced radiant heating in the water column simulated in the BIO simulation is depicted in Figure 5. Here the temperature difference between BIO and NOBIO is plotted on a vertical section at the equator during the first 6 days of the hindcast simulations after the spin-up period. The period of 6 days was chosen to restrict to the initial response before dynamical effects start to play a role. Changing the averaging period by a few days leads to a similar picture in the upper layers. However, some differences due to transient waves can nevertheless already be seen in Figure 5. The warming below 60 m does not persist while the surface structures have a longer duration and can be attributed to the changes in the solar absorption schema. Because of the enhanced absorption of light in the top layers of the ocean an enhanced warming of the upper 15 m of up to 0.2 K in BIO occurs, while the deeper ocean (30–60 m) gets cooler than without interactive biology (NOBIO). Note that the "patchiness" along the equatorial section is due to mesoscale eddies that are associated with anomalous chlorophyll concentrations. Note also that the nonuniform distribution of chlorophyll and its associated radiative surface heating leads to a reduced east-west SST gradient along the equator, which in a coupled ocean-atmosphere model would lead to a reduction of the trade winds, and in turn, to a reduction of the upwelling in the eastern equatorial Pacific. Hence, in a coupled ocean-atmosphere model, we would expect an amplification of the initial temperature signal (as, e.g., also shown by *Anderson et al.* [2007]) due to the fact that the easterly winds depend on the temperature contrast along the equator. This connection, suggested by *Bjerknes* [1966], is not included in our hindcast experiments since we focus on the oceanic effect of the temperature redistribution, leaving aside air-sea coupling.

[19] The initial redistribution of heat leads to considerable changes in the modeled circulation. First, we observe a fast evolving subsurface temperature anomaly in the central Pacific (not shown) and within the first few months of the integration a large-scale typical equatorial wave response evolves (Figure 6). The initial cold subsurface temperature
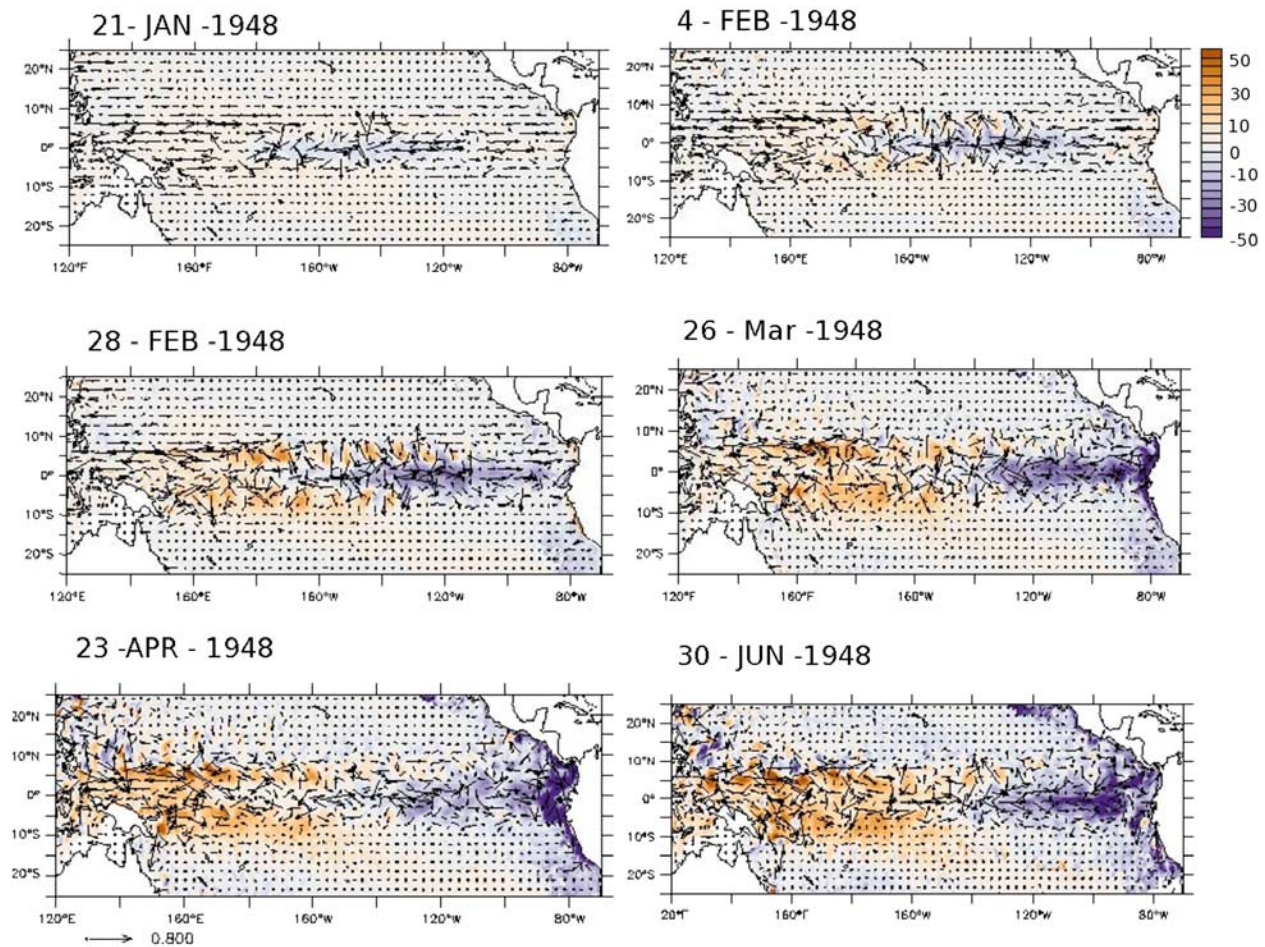
Figure 6. Snapshots of the differences in the 20° isotherm depth between the experiments BIO and NOBIO within the first 3 months of the integration in meters. The corresponding differences of the surface currents averaged over the upper 100 m are shown by the arrows in m/s. A reference arrow in the lower left corner refers to 0.8 m/s. Positive values denote regions where the 20° isotherm is deeper in the experiment BIO than in NOBIO.

anomaly between 180° and 140°W in Figure 6 and the corresponding anomalous shoaling of the 20°C isotherm of several tens of meters in BIO amplifies and begins to propagate eastward indicative of an equatorial baroclinic Kelvin wave. At the same time, off the equator subsurface warm temperature anomalies corresponding to a deepening of the thermocline begin to intensify and propagate westward, indicative of an equatorial baroclinic Rossby wave. Note that with progressing time, eddy activity related to TIWs becomes more and more incoherent in BIO and NOBIO (it is initially identical) leading to the small-scale thermocline depth anomalies and velocity differences between both simulations. Note also that with progressing time, the dynamical wave response becomes indistinguishable from changes in the seasonal cycle and the mean state in BIO and NOBIO. It finally results in a mean shoaling of the thermocline in the eastern equatorial Pacific and colder temperatures at the surface.

[20] Figure 7a shows the difference in the mixed layer depth between BIO and NOBIO. The mixed layer in the tropical Pacific is 2–18 m shallower in the BIO experiment compared to NOBIO. Note that this mixed layer shoaling is in agreement to the expected effect of the changes in heating rates in BIO vs. NOBIO [*Sweeney et al.*, 2005], that is, a near-surface warming as well as deeper cooling increases the stability of the mixed layer. Very similar results with respect to the mixed layer depth as in BIO are obtained in experiment CONSTBIO.

[21] The cooling of the eastern tropical Pacific in BIO (Figure 7b) is related to enhanced equatorial upwelling. *Sweeney et al.* [2005] showed that the shoaling of the mixed layer has a large impact on the poleward volume transports in the mixed layer of the tropical Pacific and thus on the equatorial upwelling into the mixed layer. They considered the (steady) zonal momentum budget integrated over the mixed layer (their equation (10)). Neglecting contributions from Reynolds stresses they calculated the meridional volume transport as a sum of (1) the wind driven poleward Ekman transport and (2) a flow related to the zonal pressure gradient integrated over the surface mixed layer which is partly compensating the poleward Ekman transport. Since the Ekman component is identical in BIO and NOBIO, the meridional volume transport in the mixed layer can only be changed by variations in zonal pressure gradient and/or the mixed layer depth (changing the integration depth of the zonal pressure gradients). As seen by *Sweeney et al.* [2005],
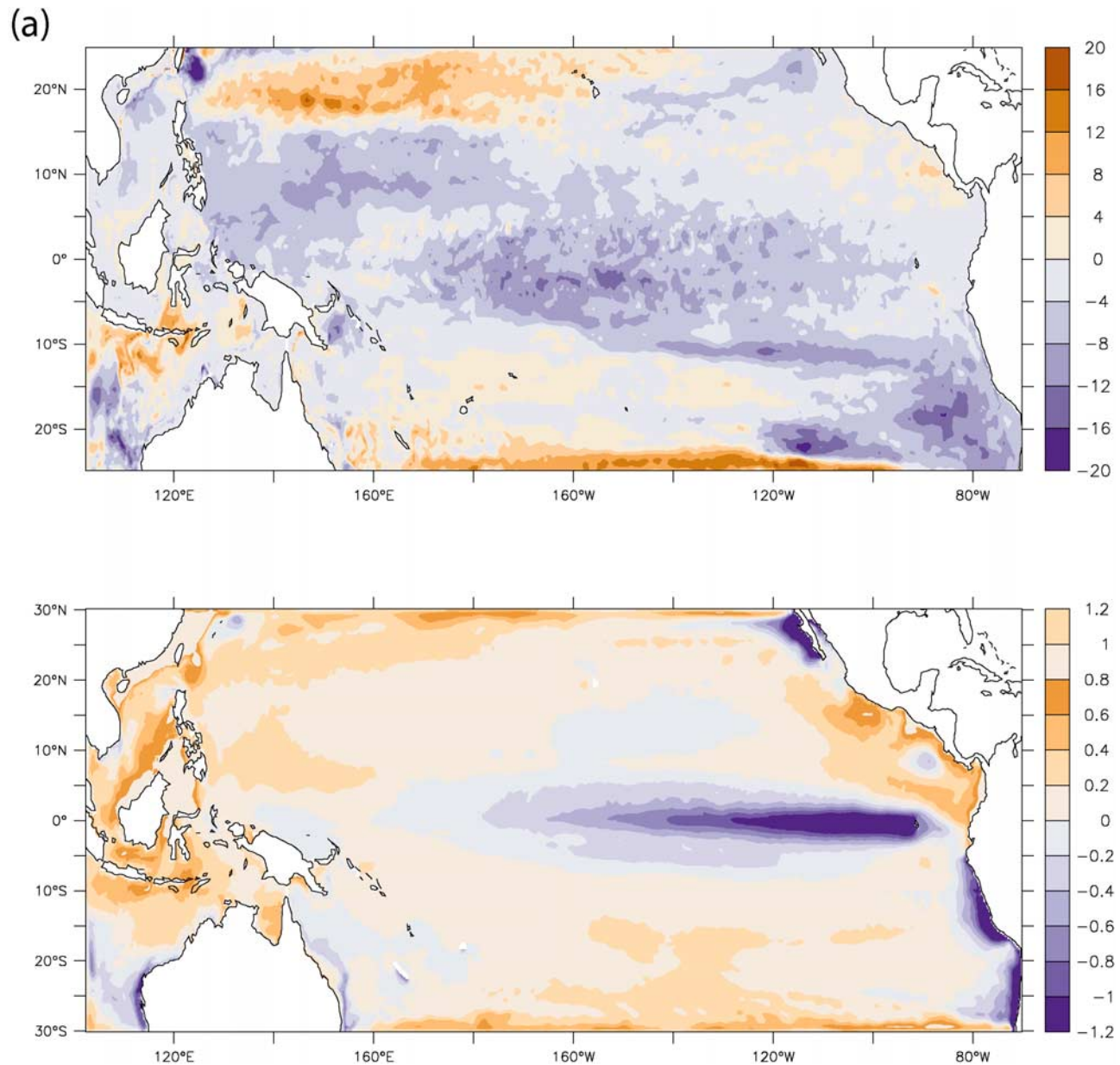
Figure 7. (a) Difference in the mixed layer depth (1948–2003) between the experiments BIO and NOBIO (MLD(BIO)-MLD(NOBIO)) in meters. The mixed layer depth is defined as the location of a vertical density change of more than 0.125 kg/m^3 relative to the surface layer. (b) Difference between the sea surface temperature (1948–2003) as modeled in BIO and NOBIO in Kelvin. Positive values denote regions with warmer temperatures in BIO compared to NOBIO.

we find that differences in the zonal pressure gradients in BIO vs. NOBIO itself are rather small (not shown) such that changes in the meridional transport are mainly due to the changes of the mixed layer depth. Thus the geostrophically balanced flow within the mixed layer, given by the flow related to the pressure gradient, is reduced in BIO with respect to NOBIO because of the shallower mixed layer, such that the net (poleward) transport is enhanced and therefore the equatorial upwelling into the mixed layer is increased.

[22]   This consideration is supported by the changes in the meridional equatorial current system. Figure 8 shows an

enhanced meridional component of the near-surface equatorial currents in BIO compared to NOBIO and thus a strengthening of the meridional shallow overturning cells. This strengthening is in turn related to stronger equatorial upwelling especially in the eastern part of the basin. Note also that the enhanced upwelling of cold waters and nutrients in BIO is more pronounced during La Niña years (not shown) when the concentration of chlorophyll in the eastern equatorial Pacific is also enhanced. This effect cannot be seen in CONSTBIO for obvious reasons, although the simulated long-term mean changes in the shallow overturning cell are similar to those in BIO. Thus one might
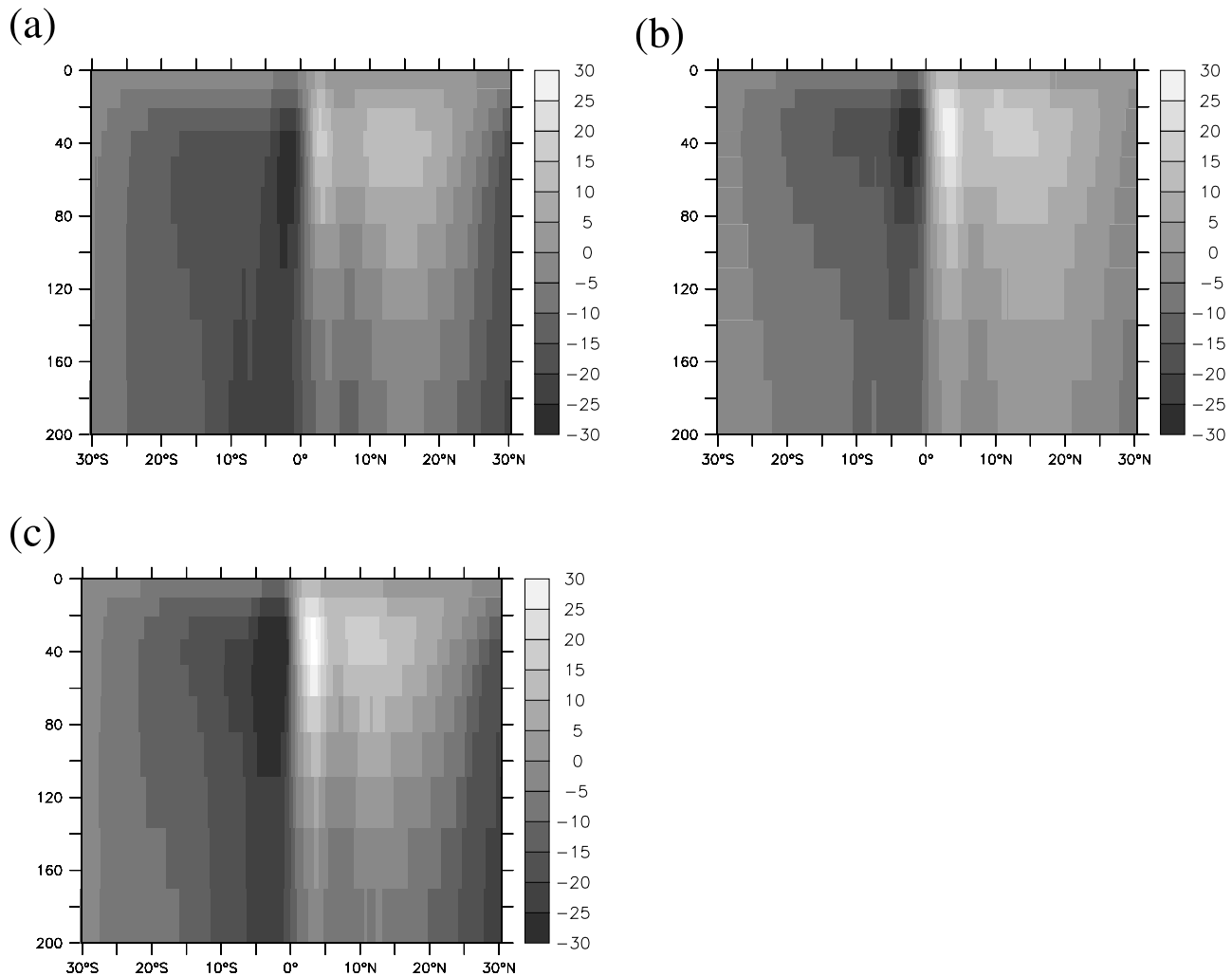
(a)

(b)

(c)

Figure 8. Simulated long-term mean (1948–2003) of the zonally integrated meridional overturning circulation in Sv in the upper 300 m for the experiments (a) NOBIO, (b) BIO, and (c) CONSTBIO.

assume that the changes in radiative heating due to ENSO-related upwelling and related chlorophyll production does not change the mean state much.

[23] The zonal currents also undergo considerable changes in BIO: Figure 9 shows the zonal currents in the experiments BIO and NOBIO along 165°E and 110°W. The South Equatorial Current (SEC) is considerably enhanced in the eastern equatorial Pacific by up to 10–15%, while the Equatorial Undercurrent (EUC) gets shallower in the BIO experiment which is due to the shoaling of the thermocline. In addition, the EUC is considerably stronger in BIO. In general, the BIO simulation reproduces many features of the observed zonal currents, as compiled for instance by *Schott et al.* [2004] (compare, e.g., their Figure 5), more realistically than the NOBIO experiment. In particular, the unrealistic surface-intensified eastward current in the western equatorial Pacific at 6°S–4°S in experiment NOBIO disappears in BIO. We also note that both horizontal and vertical current shears in the equatorial Pacific are enhanced in BIO compared to NOBIO. On the other hand, the eastward South Subsurface Counter Current (SSCC, also called Tsuchiya jets) located below about 100 m depth between 6°S–4°S at 110°W weakens considerably in

experiment BIO. Its northern counterpart, the NSCC also gets slightly weaker in BIO.

5. Simulated Interannual Variability

[24] The dominant modes of seasonal to interannual variability in the eastern tropical Pacific are the annual cycle and ENSO. Both modes interact with each other via a seasonal modulation of the interannual variance and a damping of the annual cycle strength during El Niño conditions. Coupled models still suffer from problems simulating a correct amplitude and frequency of these modes [*Bony et al.*, 2007; E. Guilyardi et al., Understanding El Niño in Ocean-Atmosphere General Circulation Models: progress and challenges, submitted to *Bulletin of the American Meteorological Society*, 2009]. However, since the surface wind stress is prescribed it is not surprising that the general agreement between simulated and observed ENSO events is very high and the correlation between the simulated and observed Niño3 time series is 0.96. The main differences between our model and observations concern the amplitude and pattern of the SST anomalies and thermocline depth, slope and circulation.
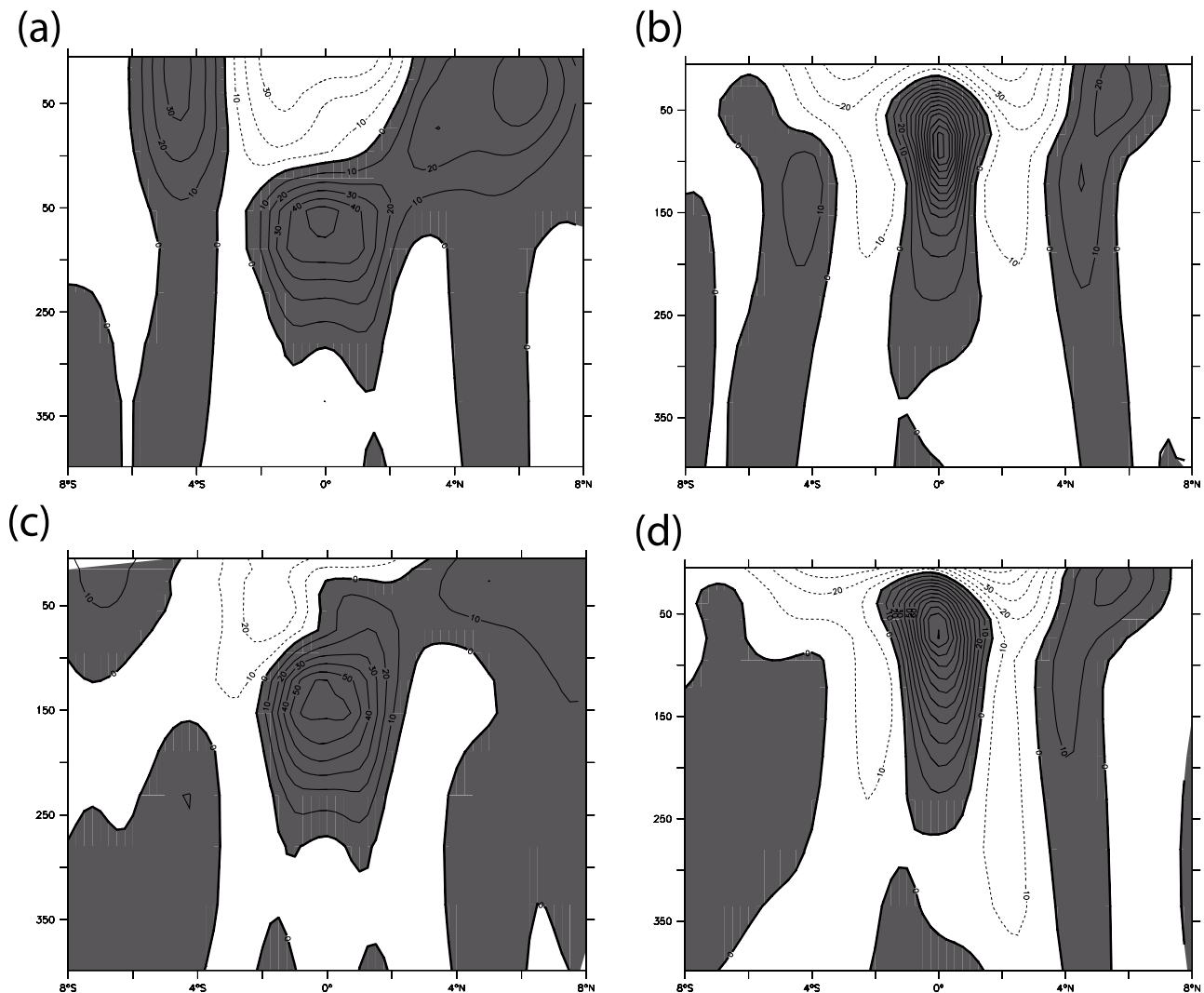
Figure 9. Long-term mean of the simulated zonal velocity at (a, c) 165°E and (b, d) 110°W from the experiments (Figures 9a and 9b) NOBIO and (Figures 9c and 9d) BIO in cm/s. The contour levels are 10 cm/s.

[25] In NOBIO the interannual SST variability is too weak compared to observations (Figure 10a). Note that the neglected variability in the surface heat fluxes might play a role for this model bias and it is also possible that the damping due to the heat flux formulation might be too strong. However, because of the shallower thermocline and mixed layer depth and the enhanced upwelling, La Niña events are more pronounced in BIO. Therefore the mean SST in the eastern part of the equatorial Pacific is reduced and the variability of the Niño3 time series is enhanced in BIO. The RMS of the monthly Niño3 SSTA time series in the experiment BIO is 0.21 K compared to 0.16 K in NOBIO. Figure 10 shows the SST anomaly in the Niño3 region smoothed with a moving average of five months from 1948–1988. Note that different mean states were subtracted and that the absolute temperature of the La Niña events is colder in BIO compared to NOBIO while the El Niño events do not tend to change much. The biologically induced cooling effect during El Niño events is on average 0.35 K in the Nino3 region while it is 1.4 K during La Niña

events. Note also that a large part of the increase in ENSO variability in BIO is already captured in the experiment CONSTBIO (RMS value of the Niño3 SSTA time series: 0.2 K).

[26] Figure 11 depicts the histograms of the mean temperature anomaly distribution in the Niño3 region for the different experiments. The observed values show a considerable positive skewness which is well known from other studies [*Burgers and Stephenson*, 1999] and implies that El Niño events can attain larger amplitudes than La Niña events. The skewness based on the observations amounts to about 0.8–0.9 [*Burgers and Stephenson*, 1999]. The same histogram for NOBIO is much narrower and the standard deviation is small adopting a value of 0.45. Furthermore, the histogram is skewed to the negative (skewness = −0.64). In BIO the histogram gets closer to the observations, the standard deviation is clearly enhanced (0.81) and the distribution is positively skewed (skewness = 0.14). The use of constant chlorophyll (CONSTBIO) leads to some improvements and larger variability (standard
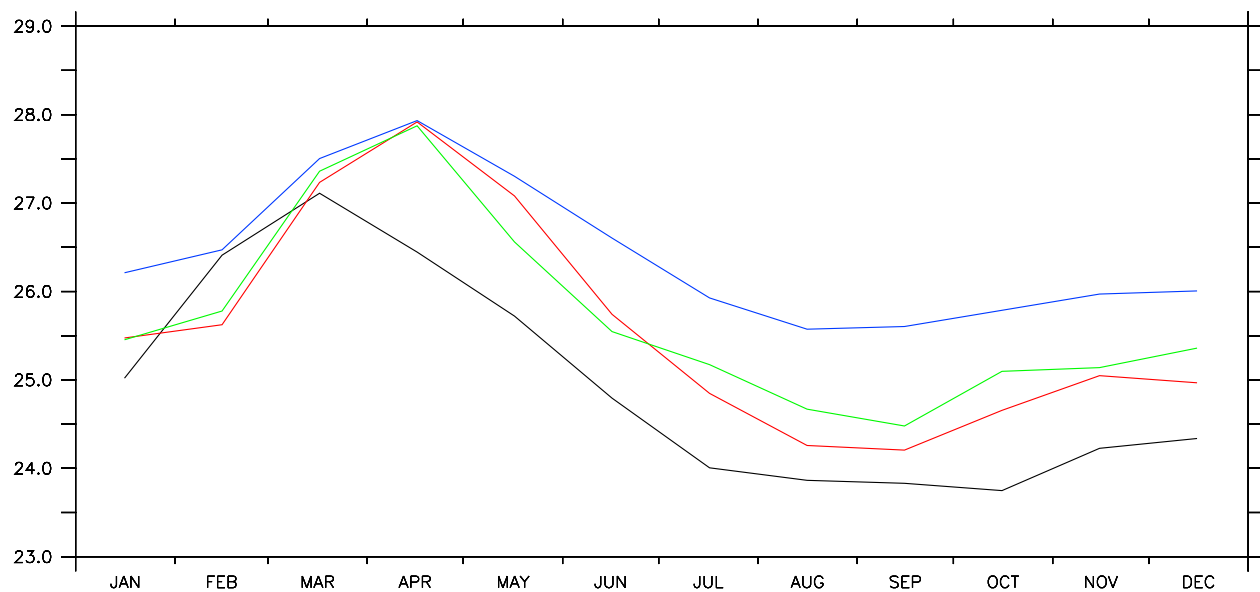
(a)
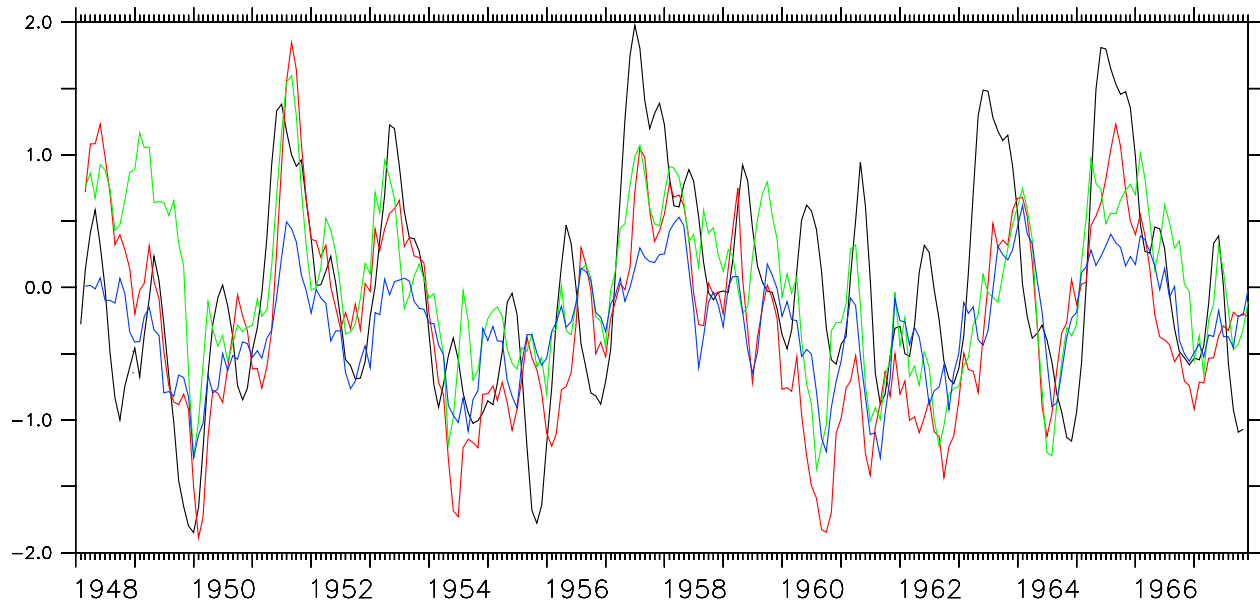
(b)

Figure 10. (a) Smoothed SST anomalies (moving average of 5 months) in the Niño3 region as modeled (colored lines) and observed (black line). The red line refers to the experiment BIO, the green line refers to CONSTBIO, and the blue line refers to NOBIO, where no biological component is included. The anomalies are calculated by subtracting the corresponding seasonal cycle of the different models. Note that the mean states are different for the different model versions. The observed sea surface temperatures (SSTs) are from *Reynolds* [1988], *Reynolds and Marsico* [1993], and *Reynolds and Smith* [1994]. (b) Mean seasonal cycle of SST in the Niño3 region as observed and modeled. The black line corresponds to observations (Reynolds), while the colored lines correspond to the different experiments (blue, NOBIO; red, BIO; green, CONSTBIO).

deviation 0.63) compared to NOBIO as well, but not to the same extent as the interactive biogeochemical model (BIO). Similar improvements are obtained for the Niño3.4 and Niño4 indices (not shown). Note, however, that considering absolute values instead of anomalies (from which different mean states have been subtracted), the La Niña events are still more pronounced even though the skewness is changed toward positive values.
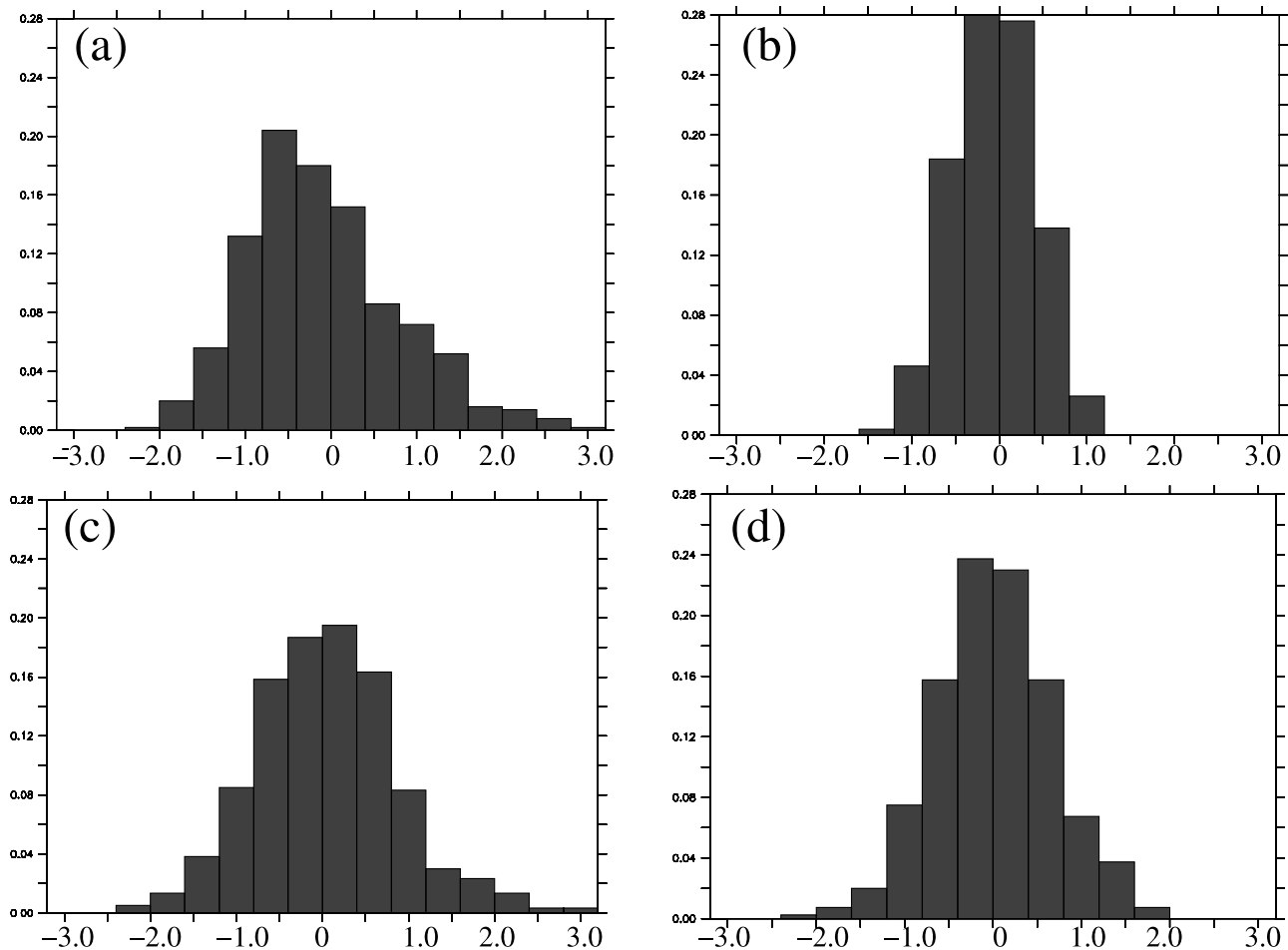
Figure 11. Normalized histograms of the SST anomalies in the Niño3 region as (a) observed and (b) simulated in NOBIO, (c) BIO, and (d) CONSTBIO. As in Figure 12, the anomalies are calculated by subtracting the corresponding mean seasonal cycles of the different models. The observed sea surface temperatures (SSTs) are taken from *Reynolds* [1988], *Reynolds and Marsico* [1993], and *Reynolds and Smith* [1994].

[27] The annual cycle of the modeled Niño3 temperature shows an offset by 1–1.5 K in NOBIO compared to the observations. This offset is reduced by approx. 1 K in BIO during autumn and winter. Additionally, the seasonal cycle is somewhat too weak in NOBIO while it is still too weak but to a lesser extent in BIO (Figure 10b). The latter changes are related to the shallower mixed layer in BIO: Surface fluxes have a stronger effect on the SST and seasonal differences are more pronounced. Furthermore, the modeled climatological SST maximum in the Nino3 region occurs in April instead of March in both simulations, even though some model studies report an earlier spring bloom in coupled models if a feedback of the biological component on the solar absorption scheme is incorporated [*Wetzel et al.*, 2006]. Besides the effect of coupling to an atmosphere in the study by *Wetzel et al.* [2006], the formulation of the biological component might cause this difference.

6. Simulated Intraseasonal Variability

[28] The main sources of high-frequency SST and surface current variations in the tropical Pacific are Tropical Instability Waves (TIWs). Such intraseasonal variability in the tropical ocean can be seen, for instance, in perturbations of the SST fronts on either side of the equatorial cold tongue. They produce SST variations on the order of 1–2 K, with periods of 20–40 days, wavelengths of 1000–2000 km, phase speeds of around 0.5 ms^{-1}. The TIWs propagate westward both north and south of the Equator with in general larger amplitudes in the northern hemisphere. TIWs are generated by instability processes associated with the large vertical and horizontal velocity shear between the westward SEC and the eastward EUC and NECC [*Masina and Philander*, 1999; *Willett et al.*, 2006]. TIWs can affect the surface chlorophyll concentration by anomalous upwelling of deep chlorophyll maxima and enhanced vertical and lateral nutrient supply. This leads to an enhanced surface warming on small scales in the presence of chlorophyll anomalies and the small-scale SST anomalies can be modified significantly. We found that the TIWs, as seen in SST, occur more frequently, last longer and extend further to the west in experiment BIO while propagation speed and period are quite similar for NOBIO and BIO.

[29] In addition, we found that intraseasonal current fluctuations associated with TIWs grow stronger in BIO. Figure 12 compares the simulated eddy kinetic energy
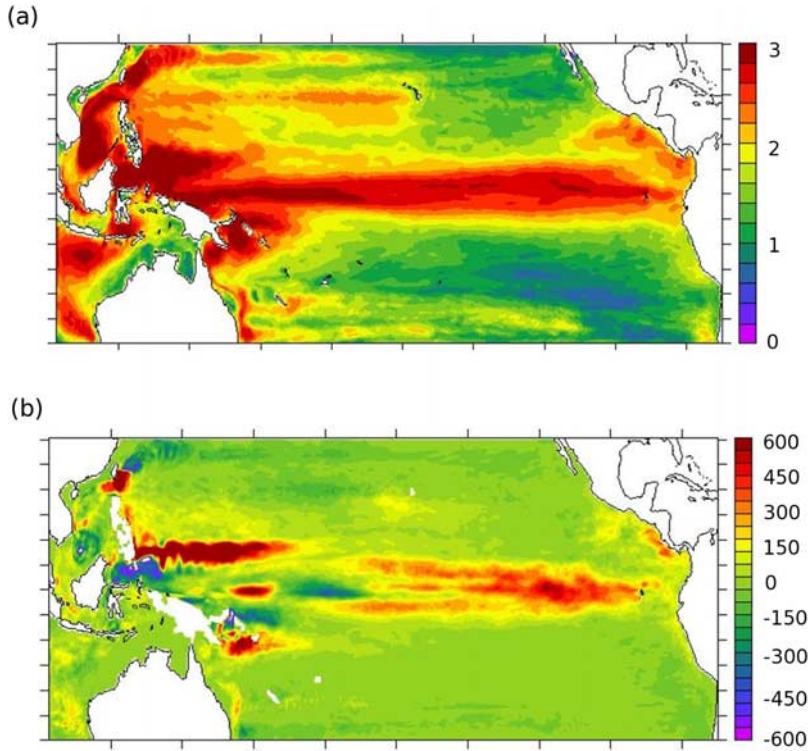
(a)

(b)

Figure 12. (a) Simulated mean near-surface eddy kinetic energy (EKE, $\overline{e} = (\overline{\mathbf{u}'\mathbf{u}'})/2$) for the period 1990–1998 for the experiment NOBIO on logarithmic scale [$\log_{10}(\text{EKE}/\text{cm}^2/\text{s}^2)$]. (b) The difference of near-surface eddy kinetic energy between the experiments BIO and NOBIO in cm^2 s^{-2}.

(EKE, $\overline{e} = (\overline{\mathbf{u}'\mathbf{u}'})/2$, where $\mathbf{u}'$ denotes deviations from the mean horizontal velocities) in experiment BIO and NOBIO. In BIO the EKE is enhanced by almost factor 2 in the equatorial Pacific relative to NOBIO. Note that this increased level of intraseasonal eddy activity is in better agreement with observational estimates of EKE, given, e.g., by drifter observations [e.g., *Lumpkin and Pazos*, 2006]. This enhancement of EKE might in turn influence the mean state in the tropical Pacific since TIWs are known to heat the cold tongue through horizontal advection [*Si*, 2008].

[30] To identify the mechanisms behind the large differences in the eddy activity in the experiment BIO and NOBIO, we consider the budget of EKE as given by Reynolds averaging:

$$\partial_t \overline{e} + \nabla_h \cdot \left(\overline{\mathbf{u}e} + \overline{\mathbf{u}'p'}\right) + \partial_z \overline{w'p}' = \overline{S} + \overline{b'w'} - \varepsilon, \qquad (1)$$

where p' denotes pressure fluctuations, b' buoyancy fluctuations and w' fluctuations of the vertical velocity. The terms on the l.h.s. of equation (1) describe changes of EKE due to advective and radiative processes which cancel out in the domain integral while the terms on the r.h.s. can be interpreted as production of EKE due to lateral shear (barotropic instability, $\overline{S} = -\overline{\mathbf{u}'\mathbf{u}'} \cdot \nabla\overline{\mathbf{u}}$), production by baroclinic instability ($\overline{b'w'}$), and dissipative processes (ε) [*Beckmann et al.*, 1994]. The primes denote the deviation from the seasonal means to exclude the seasonal signal.

[31] We also find enhanced EKE production explaining the increased levels of EKE in BIO. Figure 13 shows EKE production terms from the EKE budget due to vertical shear (often related to baroclinic instability) and horizontal shear (often related to barotropic instability). Positive values

denote transfer of energy from EKE to the mean flow for both terms while negative values show an energy transfer from the mean flow to the EKE. In both model simulations, the vertical shear of the SEC and the NECC (baroclinic instability) dominates the energy transfer in the eastern equatorial Pacific. EKE production is larger in the northern hemisphere in both experiments and is hence characterized by larger levels of EKE in that region. Off the equator, near-surface horizontal shear (barotropic) instability related to the horizontal shear between the SEC and the EUC supports the generation of EKE. In experiment BIO, the vertical shear instability gets much larger in the eastern equatorial Pacific, in agreement to the increase of EKE in experiment BIO compared to NOBIO. Note that the increase in EKE and EKE production can be explained by the enhanced vertical shear in the EUC and SEC in BIO (Figure 9). The horizontal shear production term in the eastern equatorial Pacific increases only slightly in BIO compared to NOBIO.

[32] In the western equatorial Pacific vertical shear instability also dominates the EKE production. In BIO, the EKE production by vertical shear increases only slightly while the horizontal shear production terms strongly enhances at the equator in response to the increased horizontal shear. Since TIWs are generated by baroclinic and barotropic instabilities feeding from the mean state of the model and the mean states in BIO and CONSTBIO are very similar, we expect also a similar level of EKE in CONSTBIO and BIO.

7. Summary and Discussion

[33] Recent studies as well as our ocean hindcast simulations covering the period from 1948–2003 demonstrate
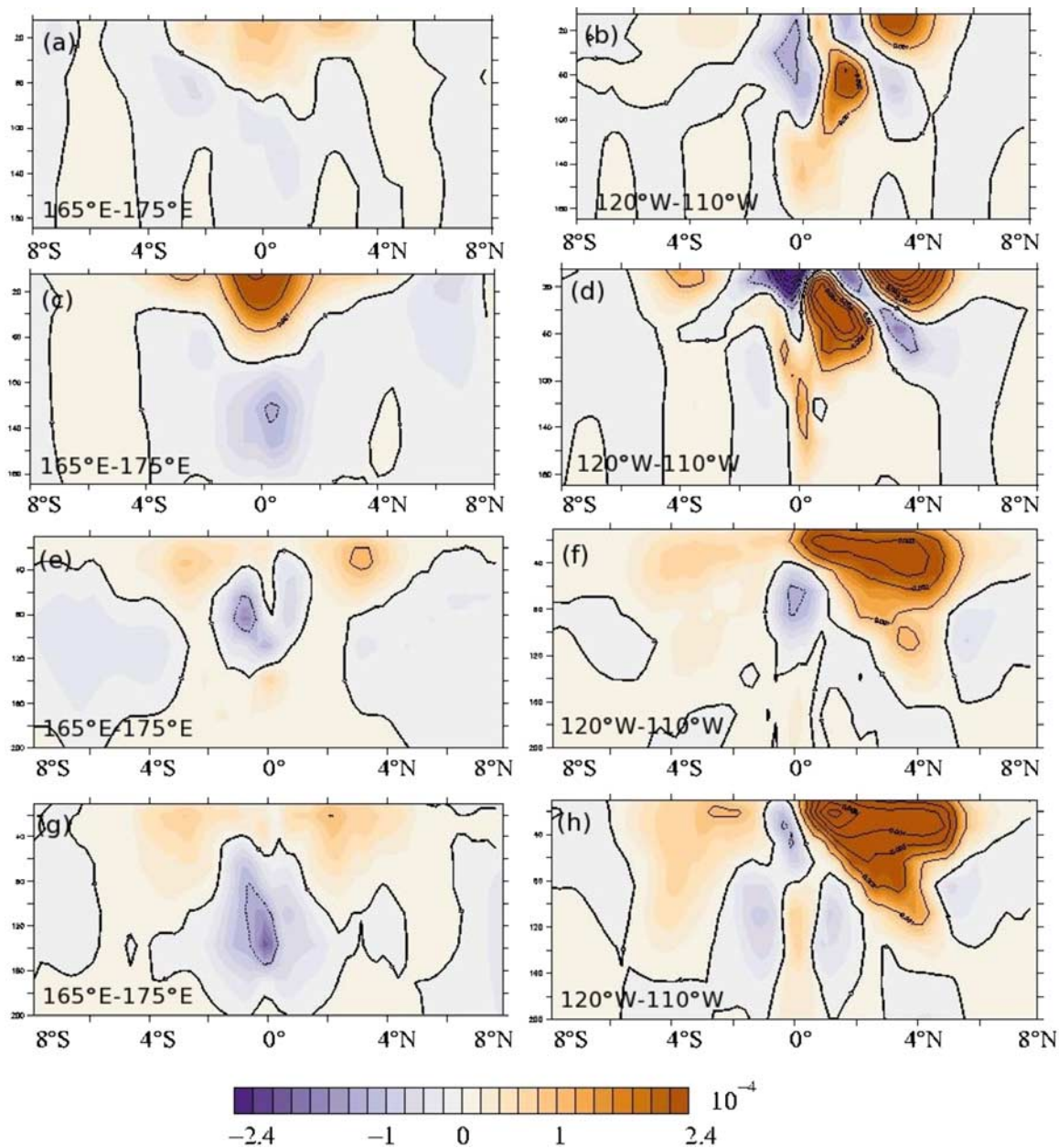
Figure 13. Energy transfer to EKE by horizontal and vertical shear (1990–1998) averaged between the longitudes indicated in the figures. Units are cm^2 s^{-3}. (a, b, c, d) EKE production due to barotropic instability ($-\overline{\mathbf{u}'\mathbf{u}'} \cdot \nabla \overline{\mathbf{u}}$) for experiments (Figures 13a and 13b) NOBIO and (Figures 13c and 13d) BIO. (e, f, g, h) Energy production due to baroclinic instability ($\overline{b'w'}$) for the experiments (Figures 13e and 13f) NOBIO and (Figures 13g and 13h) BIO in cm^2 s^{-3}. The contour levels are 0.0001 cm^2 s^{-3}. Positive values of the transfer terms denote production of EKE.

that the explicit simulation of biophysical feedbacks has considerable effects on the simulated mean climate conditions of the eastern tropical Pacific and its intraseasonal to interannual variability. We found that the biologically induced differential heating generated by increased absorption of light in the upper layers of the "chlorophyllrich" eastern equatorial Pacific generally increases the performance of our eddy-permitting ocean circulation model with respect to temperature and circulation patterns. In particular, we found that the mixed layer depth is reduced by 2–18 m in the tropical Pacific in the presence of chlorophyll because of

enhanced surface warming and subsurface cooling. In agreement with *Sweeney et al.* [2005], this is accompanied by considerable changes in the equatorial current system: The shallow overturning circulation is strongly enhanced (about 15%) because of a reduced compensation of the poleward Ekman transport by the geostrophic flow in the mixed layer. This leads to enhanced net poleward volume transport in the mixed layer and thus to an enhanced equatorial upwelling. Hence the warm bias of the SST in the eastern equatorial Pacific in our model is reduced and the SST in the upwelling region is 1.2 K cooler in the

experiment BIO compared to NOBIO. We found that this effect is considerably stronger during La Niña events and thus the interannual standard deviation of the simulated Niño3 SST time series increases from 0.45 to 0.81. This is accompanied by a change of sign in the skewness of the simulated Niño3 time series and a more pronounced seasonal cycle, all in better agreement with the observations. Moreover, also the zonal currents undergo substantial changes: the South Equatorial Current (SEC) is enhanced by up to 10–15% in the eastern equatorial Pacific, while the Equatorial Undercurrent (EUC) gets shallower by 10–15 m and stronger in the BIO experiment.

[34] These changes in the mean currents and their interannual variability are accompanied by an increase in the EKE in the equatorial Pacific by a factor of 2. This increase is related to the increase in EKE production by vertical shear within the EUC and SEC and to a lesser extent to increased horizontal shear instability.

[35] A prerequisite of a successful assessment of the effect of the biophysical coupling in our model is a realistic simulation of the near-surface chlorophyll distribution. We have used a standard NPZD model, for which we found it necessary to decrease the phytoplankton growth rate in order to prevent unrealistically high values of phytoplankton concentration and complete surface nutrient depletion in the equatorial Pacific. That choice raises the issue of how realistic the simulation is with respect to short-term (order of days) ecosystem fluctuations. It is possible that the model therefore misrepresents important feedbacks between high-frequency (eddy) activity and phytoplankton growth. However, in order to test that caveat we performed a sensitivity experiment with a different parameter setting in our NPZD model allowing for faster plankton blooms. We find that the "blooms" of the phytoplankton observed at the surface might as well originate from the upwelling of deep chlorophyll maxima and no significant differences in high-frequency chlorophyll variability occur in our simulations. Thus strong, fast phytoplankton growth might indeed be unimportant for the occurrence of sudden "blooms" observed at the surface.

[36] The simulated effects in previous model studies range from a surface warming due to the enhanced absorption of light near the surface and associated dynamical responses [e.g., *Timmermann and Jin*, 2002; *Wetzel et al.*, 2006; *Marzeion et al.*, 2005] to a surface cooling in the eastern Pacific caused by enhanced upwelling [e.g., *Manizza et al.*, 2005]. Similar uncertainties can be found for the changes in the simulated mixed layer depth in the eastern tropical Pacific. However, what appears contradictory at a first glance might be partly due to use of different clear water assumptions [*Wetzel et al.*, 2006]. Some authors compare their results to Jerlov's Type I oligotrophic water while others assume a certain basin-wide turbidity. Thus the differences in the effects of the biophysical feedbacks could be partly explained by the differences in the reference model simulation, which complicates a direct comparison of the results. Additionally, *Gnanadesikan and Anderson* [2009] as well as *Anderson et al.* [2009] show in coupled models that the details of the mean response turn out to be very dependent on the spatial region where the ocean color is perturbed.

[37] However, overall, most authors claim that the use of a biological component and the biophysical coupling brings the models closer to observations, in agreement with our finding.

[38] Our results are also different from those described in a recent CGCM study [*Lengaigne et al.*, 2007]. While in our case the strengthening of the meridional cells and a stronger EUC are accompanied by an intensification of the SEC, *Lengaigne et al.* [2007] report a weakening of the SEC. A key difference between these simulations is that winds can change in the coupled model used by *Lengaigne et al.* [2007], whereas they are prescribed in our case. Different sensitivities between coupled and uncoupled model versions were already discussed in the study by *Marzeion et al.* [2005]. Overall, however, *Lengaigne et al.* [2007] and *Manizza et al.* [2005] and our model results support the notion that an indirect dynamical response to the bio-optical coupling outweighs the direct thermal response described in the study by *Timmermann and Jin* [2002]. Thus the initial surface warming in the presence of chlorophyll is replaced by enhanced upwelling in the eastern part of the tropical Pacific and the initial signal vanishes after some months of integration.

[39] In an attempt to save computing time, we conducted an additional sensitivity experiment that uses a climatologically prescribed chlorophyll pattern instead of an explicit representation of phytoplankton. A similar approach was recently pursued by *Gildor and Naik* [2005] and *Lengaigne et al.* [2007], who found that the climate response to ocean biota can be captured reasonably well by simply prescribing a climatologically varying chlorophyll profile. Similar, but somewhat less prominent, improvements of the mean state as described above can be obtained in our model as well when the chlorophyll concentrations are held fixed in time. On the other hand, we found that the inclusion of interactive chlorophyll allows for a stronger La Niña, suggesting that the inclusion of interactive biology rather than changes in the mean state related to the spatial distribution of chlorophyll are important for ENSO simulations.

References

Anderson, W. G., A. Gnanadesikan, R. Hallberg, J. Dunne, and B. L. Samuels (2007), Impact of ocean color on the maintenance of the Pacific Cold Tongue, *Geophys. Res. Lett.*, *34*, L11609, doi:10.1029/2007GL030100.

Anderson, W., A. Gnanadesikan, and A. Wittenberg (2009), Regional impacts of ocean color on tropical Pacific variability, *Ocean Sci. Discuss.*, *6*, 243–275.

Aufdenkampe, A. K., J. J. McCarthy, C. Navarette, M. Rodier, J. Dunnea, and J. W. Murraya (2002), Biogeochemical controls on new production in the tropical Pacific, *Deep Sea Res. I*, *49*, 2619–2648.

Barnier, B., L. Siefridt, and P. Marchesiello (1995), Thermal forcing for a global ocean circulation model using a three-year climatology of ECMWF analyses, *J. Mar. Sys.*, *6*, 363–380.

Bjerknes, J. (1966), A possible response of the atmospheric Hadley Circulation to equatorial anomalies of ocean temperature, *Tellus*, *97*, 820–829.

Beckmann, A., C. W. Bönning, C. Köberle, and J. Willebrand (1994), Effects of increased horizontal resolution in a simulation of the North Atlantic Ocean, *J. Phys. Oceanogr.*, *24*, 326–344.

Bony, S., et al. (2007), Climate models and their evaluation, in *Climate Change 2007: The Physical Science Basis. Contribution of Working Group I to the Fourth Assessment Report of the Intergovernmental Panel on Climate Change*, edited by S. Solomon et al., chap. 8, pp. 623–624, Cambridge Univ. Press, Cambridge, U. K.

Burgers, G., and D. B. Stephenson (1999), The "normality" of El Niño, *Geophys. Res. Lett.*, 26, 1027–1030.

Conkright, M., S. Levitus, and T. Boyer (1994), World Ocean Atlas Volume 1: Nutrients, NOAA Atlas NESDIS, US Gov. Print. Off., Washington D.C.

Eden, C., and A. Oschlies (2006), Adiabatic reduction of circulation-related CO_2 air-sea flux biases in a North Atlantic carbon-cycle model, *Global Biogeochem. Cycles*, 20, GB2008, doi:10.1029/2005GB002521.

Gaspar, P., Y. Gregoris, and J. M. Lefevre (1990), A simple eddy kinetic energy model for simulations of the oceanic vertical mixing: Tests at station PAPA and long-term upper ocean study site, *J. Geophys. Res.*, 95, 16,179–16,193.

Gildor, H., and N. H. Naik (2005), Evaluating the effect of interannual variations of surface chlorophyll on upper ocean temperature, *J. Geophys. Res.*, 110, C07012, doi:10.1029/2004JC002779.

Gnanadesikan, A., and W. G. Anderson (2009), Ocean water clarity and the ocean general circulation in a coupled climate model, *J. Phys. Ocean.*, 39, 314–332.

Haney, R. (1971), Surface thermal boundary condition for ocean circulation models, *J. Phys. Oceanogr.*, 1, 79–93.

Jerlov, N. G. (1968), *Optical Oceanography*, Elsevier, London, U. K.

Kalnay, E., et al. (1996), The NCEP/NCAR 40-year reanalysis project, *Bull. Am. Meteorol. Soc.*, 77, 437–471.

Koehl, A., D. Dommenget, K. Ueyoshi, and D. Stammer (2006), The global ECCO 1952 to 2001, *Ocean Synth.*, Rep. 40, IFM, Hamburg, Germany.

Lengaigne, M., C. Menkes, O. Aumont, T. Gorgues, L. Bopp, J. M. André, and G. Madec (2007), Influence of the oceanic biology on the tropical Pacific climate in a coupled general circulation model, *Clim. Dyn.*, 28, doi:10.1007/s00382-006-0200-2.

Levitus, S., R. Burgett, and T. Boyer (1994), World Ocean Atlas 1994, vol 4: Temperature, NOAA Atlas NESDIS, 3–4, US Dept. of Comm., Washington, D. C.

Lewis, M. R., J. J. Cullen, and T. Platt (1983), Phytoplankton and thermal structure in the ocean: Consequences of nonuniformity in chlorophyll profile, *J. Geophys. Res.*, 88, 2565–2570.

Lewis, M. R., M. Carr, G. C. Feldman, W. Esias, and C. McClain (1990), Influence of penetrating solar radiation on the heat budget of the equatorial Pacific, *Nature*, 347, 543–546.

Lumpkin, R., and M. Pazos (2006), Measuring surface currents with Surface Velocity Program drifters: The instrument, its data, and some recent results, in *Lagarangian Analysis and Prediction of Coastal and Ocean Dynamics (LAPCOD)*, edited by A. Griffa et al., chap. 2, pp. 39–67, Cambridge Univ. Press, Cambridge, U. K.

Masina, S., and S. G. H. Philander (1999), An analysis of tropical instability waves in a numerical model of the Pacific Ocean. Part I: Spatial variability of the waves, *J. Geophys. Res.*, 104, 29–613.

Manizza, M., C. Le Quéré, A. J. Watson, and E. T. Buitenhuis (2005), Bio-optical feedbacks among phytoplankton, upper ocean physics and sea-ice in a global model, *Geophys. Res. Lett.*, 32, L05603, doi:10.1029/2004GL020778.

Marzeion, B., A. Timmermann, R. Murtugudde, and F. F. Jin (2005), Biophysical feedbacks in the tropical Pacific, *J. Clim.*, 18, 58–70.

McClain, C. R., J. R. Christian, S. R. Signorini, M. R. Lewis, I. Asanuma, D. Turk, and C. Dupouy-Douchement (2002), Satellite ocean-color observations of the tropical Pacific Ocean, *Deep Sea Res. II*, 49, 2533–2560.

McClain, C. R., G. C. Feldman, and S. B. Hooker (2004), An overview of the SeaWiFS project and strategies for producing a climate research quality global ocean bio-optical time series, *Deep Sea Res. II*, 51, 5–42.

Morel, A. (1988), Optical modeling of the upper ocean in relation to its biogenous matter content (case 1 waters), *J. Geophys. Res.*, 93, 10,749–10,768.

Murtugudde, R., J. Beauchamp, C. R. McClain, M. Lewis, and A. J. Busalacchi (2002), Effects of penetrative radiation the upper tropical ocean circulation, *J. Clim.*, 15, 470–486.

Nakamoto, S., S. P. Kumar, J. M. Oberhuber, J. Ishizaka, K. Muneyama, and R. Frouin (2001), Response of the equatorial Pacific to chlorophyll pigment in a mixed layer isopycnical ocean general circulation model, *Geophys. Res. Lett.*, 28, 2021–2024.

Oschlies, A., and V. Garcon (1998), Eddy-induced enhancement of primary production in a model of the North Atlantic Ocean, *Nature*, 394, 266–268.

Oschlies, A., and V. Garcon (1999), An eddy-permitting coupled physical-biological model of the North Atlantic. Part I: Sensitivity to advection numerics and mixed layer physics, *Global Biogeochem. Cycles*, 13, 135–160.

Ohlmann, J. C., D. A. Siegel, and C. D. Mobley (2000), Ocean radiant heating. Part I: Optical influences, *J. Phys. Oceanogr.*, 30, 1833–1848.

Pacanowski, R. C. (1992), MOM2 Documentation, User's Guide and Reference Manual, *Tech. Rep. 3*, Ocean group, Geophys. Fluid Dyn. Lab., Princeton, N. J.

Pennington, J. T., K. L. Mahoney, V. S. Kuwahara, D. D. Kolber, R. Calienes, and F. P. Chavez (2006), Primary production in the eastern tropical Pacific: A review, *Prog. Oceanogr.*, 69, 2–4, 285–317.

Penta, B., Z. Lee, R. M. Kudela, S. L. Palacios, D. J. Gray, J. K. Jolliff, and I. G. Shulman (2008), An underwater light attenuation scheme for marine ecosystem models, *Opt. Express*, 21, 16,581–16,591.

Reynolds, R. W. (1988), A real-time global sea surface temperature analysis, *J. Clim.*, 1, 75–86.

Reynolds, R. W., and D. C. Marsico (1993), An improved real-time global sea surface temperature analysis, *J. Clim.*, 6, 114–119.

Reynolds, R. W., and T. M. Smith (1994), Improved global sea surface temperature analyses using optimum interpolation, *J. Clim.*, 7, 929–948.

Ryan, J. P., I. Ueki, Y. Chao, H. Zhang, P. S. Polito, and F. P. Chavez (2006), Western Pacific modulation of large phytoplankton blooms in the central and eastern equatorial Pacific, *J. Geophys. Res.*, 111, G02013, doi:10.1029/2005JG000084.

Sathyendranath, S., A. D. Gouveia, S. R. Shetye, P. Ravindran, and T. Platt (1991), Biological control of the surface temperature in the Arabian Sea, *Nature*, 349, 54–56.

Schott, F. A., J. P. McCreary, and G. C. Johnson (2004), Shallow overturning circulations of the tropical-subtropical oceans, *Geophys. Monogr. AGU*, 137, 261–304.

Seager, R., M. B. Blumenthal, and Y. Kushnir (1995), An advective atmospheric mixed layer model for ocean modeling purposes: Global simulation of surface heat fluxes, *J. Clim.*, 8, 1951–1964.

Si, A. (2008), Interannual variations of the tropical ocean instability wave and ENSO, *J. Clim.*, 21, 3680–3686.

Stevens, D. P. (1990), On open boundary conditions for three dimensional primitive equation ocean circulation models, *Geophys. Astrophys. Fluid Dyn.*, 51, 103–133.

Strutton, P. G., and F. P. Chavez (2004), Biological heating in the equatorial Pacific: Spatial and temporal variability, *J. Clim.*, 17, 1097–1109.

Sweeney, C., A. Gnanadesikan, S. M. Griffies, M. J. Harrison, A. J. Rosati, and B. L. Samuels (2005), Impacts of shortwave penetration depth on large-scale ocean circulation and heat transport, *J. Phys. Ocean.*, 35, 1103–1119.

Timmermann, A., and F.-F. Jin (2002), Phytoplankton influences on tropical climate, *Geophys. Res. Lett.*, 29(23), 2104, doi:10.1029/2002GL015434.

Vialard, J., C. Menkes, D. L. T. Anderson, and M. A. Balmaseda (2003), Sensitivity of Pacific ocean tropical instability waves to initial, *J. Phys. Ocean.*, 33, 105–121.

Wetzel, P., E. Maier-Reimer, M. Botzet, J. Jungclaus, N. Keenlyside, and M. Latif (2006), Effects of ocean biology on the penetrative radiation in a coupled climate model, *J. Clim.*, 19, 3973–3987.

Willett, C. S., R. R. Leben, and M. F. Lavín (2006), Eddies and tropical instability waves in the eastern tropical Pacific: A review, *Progr. Oceanogr.*, 69, 218–238.

Zhang, R., A. J. Busalacchi, X. Wang, J. Ballabrera-Poy, R. G. Murtugudde, E. C. Hackert, and D. Chen (2009), Role of ocean biology-induced climate feedback in the modulation of El Niño-Southern Oscillation, *Geophys. Res. Lett.*, 36, L03608, doi:10.1029/2008GL036568.

———————————

H. Dietze, Marine Biogeochemie, Leibniz-Institut für Meereswissenschaft, Düsternbrooker Weg 20, D-24105 Kiel, Germany. (hdietze@ifm-geomar.de)

C. Eden and U. Löptien, Ozeanzirkulation und Klimadynamik, Leibniz-Institut für Meereswissenschaften, Düsternbrooker Weg 20, D-24105 Kiel, Germany. (ceden@ifm-geomar.de; uloeptien@ifm-geomar.de)

A. Timmermann, IPRC, SOEST, University of Hawai'i at Manoa, 2525 Correa Road, Honolulu, HI 96822, USA. (axel@hawaii.edu)